

Spe
647

Dead-End Pore Volume and Dispersion in Porous Media

K. H. COATS
JUNIOR MEMBER AIME
B. D. SMITH*

JERSEY PRODUCTION RESEARCH CO.
TULSA, OKLA.

ABSTRACT

Experiments in which calcium chloride displaced sodium chloride from four cores showed the extent of asymmetry in the resulting effluent concentration profiles. These results provided a check on how validly the mixing process is modeled by a differential (i.e., not finite-stage) capacitance mathematical model.

The effluent concentration profile from two consolidated cores exhibited considerable asymmetry, while two unconsolidated cores yielded nearly symmetrical profiles. All runs resulted in breakthrough of the 50 per cent concentration significantly before one pore volume was injected. In addition, velocity appreciably affected the effluent concentration profile from a Torpedo sandstone core.

The differential capacitance model matched the data significantly better than a simple diffusion model. The capacitance model allows determination of the amount of dead-end pore space in a porous matrix and the effect of velocity on the rate of diffusion into this space. An experimental program yielding insight into the physical validity of the capacitance effect is described.

INTRODUCTION

Axial dispersion — the mixing accompanying the flow of miscible fluids through porous media — has been the subject of many relatively recent studies¹⁻¹³ and a comprehensive review of the topic has been given by Perkins and Johnston.¹⁴ This dispersion is of practical interest in studies of the miscible displacement process, fixed-bed chemical reactors, and the adsorption of solutes from a flowing stream onto the surface of a porous medium. In the latter case, the effect of dispersion must be considered when adsorption parameters are determined from the nature of concentration profiles.

In general, early studies of dispersion assumed applicability of a simple diffusion equation and were concerned with correlation of the experimentally determined "effective" diffusion coefficient with

system properties over a large range of the latter.

Recent investigators⁹⁻¹³ have been concerned with the deviations between the asymmetrical effluent concentration profiles observed and the symmetrical ones predicted by the diffusion model.

In the present study, effluent concentration profiles were obtained from consolidated and unconsolidated cores. These profiles were compared with those predicted by a differential (i.e., not finite-stage) capacitance model. Solutions to the simple diffusion model, for three sets of boundary conditions, were compared with one another and with the experimental profiles.

SUMMARY OF PREVIOUS WORK

The reader is referred to Perkins and Johnston¹⁴ for an extensive review of studies of dispersion in porous media. Many investigators have employed the simple diffusion model characterized by Eq. 1 below:

$$D \frac{\partial^2 C}{\partial x^2} - v \frac{\partial C}{\partial x} = \frac{\partial C}{\partial t} \dots \dots \dots (1)$$

The dispersion coefficient D for unconsolidated systems is correlated by

$$D = 1.75 v d_p \dots \dots \dots (2)$$

for $2 < v d_p / D_o < 50$, where v is interstitial velocity and d_p is particle diameter. Since heterogeneity of the sand pack affects the mixing, this equation is also expressed as

$$D = 0.5 v \sigma d_p \dots \dots \dots (3)$$

where σ is proportional to the degree of heterogeneity and is about 3.5 for random packs of unconsolidated sand.¹⁴ Eq. 3 holds for $2 < \frac{v d_p \sigma}{D_o} < 50$. For a homogeneous (regular) type of packing, σ should be 1 or less.⁶ Aris and Amundson⁶ and Carberry and Bretton⁷ consider σ to be the number of particle lengths per mixing cell in the finite-stage model. Data from consolidated cores indicate σd_p to be about 0.36 cm for outcrop rocks, Torpedo sandstone having a reported value of 0.17 cm.¹⁵ For $v d_p / D_o$ less than about 2, the effect of molecular diffusion must be considered and the total dispersion coefficient

Original manuscript received in Society of Petroleum Engineers office Sept. 5, 1963. Revised manuscript received Jan. 19, 1964. Paper presented at Annual SPE Fall Meeting held Oct. 6-9, 1963 in New Orleans.

*Presently an associate professor, School of Chemical Engineering, Purdue U., Lafayette, La.

¹References given at end of paper.

cient D is the sum of the molecular term $D_0/F\phi$ and the convective term on the right side of Eq. 3. The value of $1/F\phi$ is generally about 0.7 for unconsolidated media, significantly less for consolidated media.

Several writers have proposed dispersion models which differ from the simple diffusion Eq. 1. Aris and Amundson, and Carberry and Bretton discuss a finite-stage model in which a porous medium is viewed as a series of mixing cells, each having uniform composition. For a small number of such cells in series, the calculated concentration profile is asymmetrical, while the profile for a large number of cells approaches the symmetrical, normal distribution predicted by Eq. 1 (for large γ). This mixing cell model and Eq. 1 give similar concentration profiles provided D in 1 obeys

$$\frac{v d_p}{D} = \frac{2}{\sigma} \dots \dots \dots (4)$$

Thus, if σ changes very slowly with velocity then the dispersion coefficient D should vary linearly with velocity. As mentioned above, this behavior is experimentally observed.

Deans¹² has proposed a finite-stage model which consists of the above-mentioned mixing cell model augmented by terms accounting for mass transfer from the flowing stream into stagnant volume. This "capacitance" model has three parameters: number of stages, amount of stagnant volume, and rate constant for the mass transfer to the latter. This model is discussed further.

Gottschlich¹³ recently presented a "film" model which is differential (as opposed to finite-stage) and which treats bed capacitance by supposing the stagnant volume to occur as a thin film over the rock or sand surface. Mass transfer into this film is governed by the diffusion equation, $D_0 \frac{\partial^2 C}{\partial Z^2} = \frac{\partial C}{\partial t}$, where Z is distance within the film. This model also has three parameters: dispersion coefficient D , amount of liquid in the film, and a parameter involving film thickness and diffusion coefficient.

Turner⁹ and van Deemter, *et al.*,² discuss the differential capacitance model, employed in this study, in connection with pulse or periodic input concentration. Lapidus and Amundson¹ give a double-integral form of solution for this model.

MATHEMATICAL MODELS EMPLOYED IN THIS STUDY

The effluent concentration data obtained in this study are compared with the standard diffusion model, a differential form of Deans' finite-stage capacitance model, and the differential capacitance model described in this section.

DIFFUSION MODEL

The standard diffusion model for the step-input type of experiment is constituted by a number of

solutions to Eq. 1, each solution corresponding to a different selection of boundary conditions.* Three such solutions are considered here. The most general treatment of the boundary conditions has been given by Bischoff and Levenspiel.¹⁰ They considered a system composed of a packed bed preceded by an entrance section, denoted by subscript a , and followed by an exit chamber, denoted by subscript b . If x_0 denotes the position in the entrance section at which concentration is step-changed, o the inlet face of the core, and L the end of the core, then their boundary conditions are:

$$\text{At } x = x_0, C_a = C_0; \dots \dots \dots (5)$$

$$\text{at } x = 0, v C_a - D_a \frac{\partial C_a}{\partial x} = v C - D \frac{\partial C}{\partial x}, \text{ and } C_a = C; \dots \dots (6)$$

$$\text{at } x = L, v C - D \frac{\partial C}{\partial x} = v C_b - D_b \frac{\partial C_b}{\partial x}, \text{ and } C = C_b \dots \dots (7)$$

Perhaps the most widely employed specialization of conditions 5, 6 and 7 is:

$$\text{at } x = 0, C = C_0$$

and

$$\text{as } x \rightarrow \infty, C(x,t) \rightarrow 0 \dots \dots (8)$$

Eqs. 8 presuppose the validity of conditions 5 when $x_0 = 0$ and the insensitivity of the solution to the existence or non-existence of a core extension from L to infinity. Aris and Amundson⁶ note that when the entrance section is ignored (i.e., $x_0 = 0$), Eq. 6 is the proper condition and the conditions 8 should read

$$\text{at } x = 0, v C_0 = v C - D \frac{\partial C}{\partial x}$$

and

$$\text{as } x \rightarrow \infty, C(x,t) \rightarrow 0 \dots \dots (9)$$

Eqs. 9 comprise the second set of boundary conditions considered here. Brenner¹¹ employs Danckwerts'¹⁹ reasoning in treating the case of a finite core with the conditions

$$\text{at } x = 0, v C_0 = v C - D \frac{\partial C}{\partial x}$$

and

$$\text{at } x = L, \frac{\partial C}{\partial x} = 0 \dots \dots (10)$$

The second of conditions 10 derives from 7, with the stipulation that $D_b \ll D$ (i.e., mixing in the exit chamber is small compared with mixing in the core).

*Initial condition is $C(x,0) = 0$.

The solution to Eq. 1 for conditions 8 is well known:

$$\frac{C}{C_0} = \frac{1}{2} \left[\operatorname{erfc} \left(\frac{\sqrt{\gamma}}{2} \frac{y-1}{\sqrt{I}} \right) + e^{\gamma y} \operatorname{erfc} \left(\frac{\sqrt{\gamma}}{2} \frac{y+1}{\sqrt{I}} \right) \right] \dots \dots \dots (11)$$

Approximation of the second term in the brackets* gives

$$\frac{C}{C_0} = \frac{1}{2} \operatorname{erfc} \left(\frac{\sqrt{\gamma}}{2} \frac{y-1}{\sqrt{I}} \right) + \frac{\sqrt{I}}{\sqrt{\pi \gamma} (y+1)} e^{-\frac{\gamma}{4I} (y-1)^2} \dots \dots \dots (12)$$

which gives an error in C/C_0 of less than 0.5 per cent for $\gamma > 50$.

The solution to Eq. 1 for conditions 9 is given by Brenner¹¹ and derived in a somewhat more straightforward manner in Appendix A as

$$\begin{aligned} \frac{C}{C_0} = & \frac{1}{2} \left[\operatorname{erfc} \left(\frac{\sqrt{\gamma}}{2} \frac{y-1}{\sqrt{I}} \right) - e^{\gamma y} \operatorname{erfc} \left(\frac{\sqrt{\gamma}}{2} \frac{y+1}{\sqrt{I}} \right) \right] \\ & - \frac{\gamma}{2} (y+1) e^{\gamma y} \operatorname{erfc} \left(\frac{\sqrt{\gamma}}{2} \frac{y+1}{\sqrt{I}} \right) \\ & + \sqrt{\frac{\gamma I}{\pi}} e^{-\frac{\gamma}{4I} (y-1)^2} \dots \dots \dots (13) \end{aligned}$$

Approximation¹⁸ of the term $\operatorname{erfc} \left(\frac{\sqrt{\gamma}}{2} \frac{y+1}{\sqrt{I}} \right)$ reduces 13 to

$$\frac{C}{C_0} = \frac{1}{2} \operatorname{erfc} \left(\frac{\sqrt{\gamma}}{2} \frac{y-1}{\sqrt{I}} \right) - \frac{\sqrt{I}}{\sqrt{\pi \gamma} (y+1)} e^{-\frac{\gamma}{4I} (y-1)^2} \left(1 - 2 \frac{I}{I+1} \right) \dots \dots (14)$$

which possesses the same accuracy as 12.

Brenner's solution to Eq. 1 for conditions 10 appears to be in error in its asymptotic form for large γ (say > 50). The correct form of his Eq. 26 is, for large γ and at $y = 1$,

$$\begin{aligned} \frac{C}{C_0} = & \frac{1}{2} \operatorname{erfc} \left(\frac{\sqrt{\gamma}}{2} \frac{1-1}{\sqrt{I}} \right) - \frac{\sqrt{I}}{\sqrt{\pi \gamma} (1+1)} e^{-\frac{\gamma}{4I} (1-1)^2} \\ & \left(1 - 6 \frac{I}{1+1} - 2 \frac{I^2}{(1+1)^2} \right), \dots \dots \dots (15) \end{aligned}$$

which is accurate to 0.2 per cent for $\gamma > 50$ and to 0.05 per cent for $\gamma > 100$. Brenner's version of 15 has (+4) in place of (-2) in the last term. Error in his version is indicated by the steady growth of the error in his asymptotic form (see his Table I) from zero for $\gamma = 16$ to 0.0024 at $\gamma = 40$.

Eqs. 12, 14 and 15 are the three versions of the diffusion model employed in this study. A minor

addition is made to these equations by allowing the existence of an amount of stagnant volume into which diffusion is negligibly slow. This is easily accomplished by replacing l in the solutions by l/f , where f is the fraction of the total pore volume occupied by mobile fluid.

Quantitative comparison of Eqs. 12, 14 and 15 is rather difficult by inspection. One measure of comparison is the value of effluent concentration at one pore volume injected. At $y = l = 1$, the three solutions 12, 14 and 15 become, respectively,

$$\frac{C}{C_0} = \frac{1}{2} + \frac{1}{2\sqrt{\pi \gamma}} \dots \dots \dots (16)$$

$$\frac{C}{C_0} = \frac{1}{2}, \dots \dots \dots (17)$$

and

$$\frac{C}{C_0} = \frac{1}{2} + \frac{5}{4} \frac{1}{\sqrt{\pi \gamma}} \dots \dots \dots (18)$$

For a γ value of 100, Eqs. 16 and 18 give corresponding C/C_0 values 6 per cent and 14 per cent

TABLE I — C/C_0 AT $x=L$ FOR STEP-INPUT EXPERIMENT

γ	l	Infinite Bed Eq. 12	Infinite Bed Eq. 14	Finite Bed Eq. 15
50	.7	.0445	.0352	.0508
	.8	.1531	.1295	.1756
	.9	.3339	.2974	.3786
	1.0	.5399	.5000	.5997
	1.1	.7187	.6848	.7789
	1.2	.8455	.8217	.8944
	1.3	.9224	.9079	.9562
100	1.45	.9759	.9703	.9913
	.8	.0651	.0561	.0736
	.9	.2495	.2270	.2771
	1.0	.5282	.5000	.5705
	1.1	.7722	.7508	.8102
	1.2	.9138	.9027	.9366
	1.3	.9735	.9692	.9835
150	.8	.0300	.0261	.0337
	.9	.1959	.1799	.2154
	1.0	.5239	.5000	.5576
	1.1	.8118	.7962	.8394
	1.2	.9495	.9436	.9618
	1.3	.9903	.9889	.9938
	200	.85	.0572	.0514
.9		.1574	.1454	.1722
.95		.3215	.3036	.3460
1.0		.5199	.5000	.5499
1.05		.7049	.6876	.7332
1.1		.8423	.8303	.8637
1.15		.9264	.9195	.9398
300	1.225	.9814	.9792	.9862
	.9	.0555	.0981	.1146
	.95	.2783	.2646	.2970
	1.0	.5163	.5000	.5407
	1.05	.7384	.7252	.7602
	1.1	.8866	.8788	.9005
	1.2	.9886	.9874	.9911
390	.9	.0754	.0703	.0817
	.95	.2480	.2367	.2634
	1.0	.5143	.5000	.5357
	1.05	.7634	.7523	.7815
	1.10	.9143	.9087	.9242
	1.175	.9890	.9880	.9911

*See Ref. 18, page 483.

larger than 0.5. Table 1 lists effluent concentration as a function of injected pore volumes as computed from Eqs. 12, 14 and 15 for a range of γ values.

DEANS' CAPACITANCE MODEL

In an attempt to account for the tailing or asymmetry noted in effluent concentration profiles, Deans¹² modified the mixing cell model to include diffusion or mass transfer into stagnant volume. Deans gives the differential form of his model (for small mixing cell length) as

$$-v \frac{\partial C}{\partial x} = f \frac{\partial C}{\partial t} + (1-f) \frac{\partial C^*}{\partial t}, \dots (19)$$

where C^* is concentration in the stagnant volume, and

$$(1-f) \frac{\partial C^*}{\partial t} = K (C - C^*) \dots (20)$$

With the definitions $a = KL/v$, $Y = ay$ and $Z = \frac{af}{1-f} (J - y)$, Eqs. 19 and 20 reduce to

$$- \frac{\partial C}{\partial Y} = \frac{\partial C^*}{\partial Z} = C - C^*, \dots (21)$$

to which the solution for a step-change in feed concentration (from zero to C_0) is²⁰

$$\frac{C}{C_0} = 1 - e^{-Z} \int_0^Y e^{-x} I_0(2\sqrt{xZ}) dx \dots (22)$$

This solution is only valid for $Z > 0$; C/C_0 is zero for $Z < 0$. Since Eq. 22 yields

$$\frac{C}{C_0} = e^{-Y} \dots (23)$$

for $Z = 0$, and since $l = f$ when Z is zero, Eq. 22 predicts that effluent concentration will remain zero until $l = f$, at which time all concentrations between zero and e^{-Y} simultaneously appear. A second property of the model (Eq. 22) is that at $Z = Y$ ($l = 1$),

$$\frac{C}{C_0} = \frac{1}{2} + \frac{1}{2} e^{-2Y} I_0(2Y), \dots (24)$$

and approximation of the Bessel function $I_0(2Y)$ for $Y > 2$ yields

$$\frac{C}{C_0} = \frac{1}{2} + \frac{1}{4\sqrt{\pi a}} \dots (25)$$

In Eq. 25, Y has been replaced by (a) since $Y = a$ when effluent concentration is considered ($y = 1$). Thus use of Eq. 24, along with an experimental value of effluent C/C_0 at one pore volume injected, yields the value of the rate group (a) directly. Graphical representation of the solution 22 is available in the literature²¹ for determination of C/C_0 at l values other than f and unity.

The reduction of Eq. 22, for large Z and Y , to a form nearly identical to the diffusion model solutions is given in Appendix B.

DIFFERENTIAL CAPACITANCE MODEL

If the diffusion Eq. 1 is augmented by terms accounting for stagnant volume, the result is

$$D \frac{\partial^2 C}{\partial x^2} - v \frac{\partial C}{\partial x} = f \frac{\partial C}{\partial t} + (1-f) \frac{\partial C^*}{\partial t}, \dots (26)$$

and

$$(1-f) \frac{\partial C^*}{\partial t} = K (C - C^*), \dots (27)$$

where Eq. 27 presupposes a first-order mass transfer process.

This set of equations is solved, for boundary conditions 9, in Appendix C with the result,

$$\frac{C}{C_0} = \frac{2e}{\pi} \int_0^\infty \frac{e^{\frac{Y}{2}(1-\sqrt{p}) \cos \frac{\phi}{2}}}{a_1^2 + a_2^2} \left[a_1 \cos(ZJ-w) + a_2 \sin(ZJ-w) \right] dZ \dots (28)$$

Terms in Eq. 28 are defined in Appendix C. An analytical solution to Eqs. 26 and 27 has been given by Lapidus and Amundson¹ in the form of a double integral over time. The form of the solution given in Appendix C is somewhat more amenable to numerical evaluation in that a single integral is involved.

Properties of this model are more easily discernible from dimensionless forms of Eqs. 26 and 27:

$$\frac{1}{\gamma} \frac{\partial^2 C}{\partial y^2} - \frac{\partial C}{\partial y} = f \frac{\partial C}{\partial I} + (1-f) \frac{\partial C}{\partial I}, \dots (29)$$

and

$$(1-f) \frac{\partial C^*}{\partial I} = a (C - C^*) \dots (30)$$

For sufficiently small velocity, the rate group (a) will be large and the mass transfer process will be essentially instantaneous. The model reduces to Eq. 1 in this case, and the solution is given by Eq. 14. For sufficiently large velocity, the rate group (a) will be negligibly small and the model again reduces to Eq. 1, with solution 14, except that J must replace l in the latter two equations.

EXPERIMENTAL PROCEDURE

Step-input experiments were conducted with cores of Wausau sand, Ottawa sand, Torpedo sandstone and Alundum. Five per cent calcium chloride was injected into the cores, which initially contained 5 per cent sodium chloride. Small effluent samples were collected in weighed vials and the fluid volumes were determined by weight difference. Density, as a function of composition of the sodium and calcium chloride solutions, was taken into account. Calcium content was determined by the Versine or EDTA titration method.

The possible occurrence of adsorption or ion

exchange was investigated by batch experiments wherein sand or crushed rock was contacted with the calcium chloride with and without sodium chloride initially present. Analyses for calcium content as a function of time showed that no discernible change in concentration occurred over the period of a day. The absence of adsorption effects was also indicated by the breakthrough of the 0.5 C/C₀ point in the flow tests prior to one pore volume injected. If adsorption had been significant, the breakthrough of solute would have been delayed, with the 0.5 C/C₀ point appearing after one pore volume injected.

Pore volumes of each core were carefully obtained by expanding air into the evacuated cores and correcting the calculated pore volumes for non-core system volume. Both authors measured this non-core volume independently by injecting water with a calibrated syringe and obtained the same results. Each end-plate in the Torpedo sandstone core contained 0.4 cc of "non-core" volume while the system volume downstream of the exit valve (to the end of the short outlet line) was 1 cc. Collected volumes were corrected for non-core volume in determining pore volumes injected (*I*). This non-core volume is not part of the hypothesized stagnant (core) volume discussed herein. The pore volumes are believed accurate to within ±0.2 cc.

The possibility of adsorption as well as viscosity effects was further examined by comparing the effluent concentration profiles for sodium chloride displaced by calcium chloride, and vice versa. The resulting profiles were virtually identical.

The unconsolidated cores were prepared by pouring the sand slowly into the lucite tube while agitating with a hand vibrator. The consolidated cores were fused to lucite tubes under a uniform external pressure (ends and circumference) of 1,000 psi at a temperature of 276F. The pressure was maintained at 1,000 psi as the cores were cooled to room temperature over the period of one day. Distribution plates with two concentric rings and four rays were employed at the core inlet and outlet. Fluid feeding was attained by nitrogen pressure, maintained through a constant head device over the surface of the solution in a four-liter, lucite feed tank. Flow rate was measured by timing the collection of core effluent samples.

Table 2 gives core properties, and Table 3 lists the run variables. The experimental effluent concentration curves are plotted in Figs. 1 through 7. The effluent sample sizes were about 0.006, 0.01, 0.02, 0.016, 0.03, 0.03 and 0.015 pore volumes for runs 1 through 7 respectively.

TABLE 3 — RUN VARIABLES

Run	Core	v_i , cm/sec	v_i , ft/day	γ	D , sq cm/sec
1	Torpedo	.009	25.6	370	.00057
2	Torpedo	.0525	150	302	.00409
3	Torpedo	.202	575	212	.02240
4	Alundum	.0163	46.5	730	.00045
5	Alundum	.192	546	780	.0050
6	Ottawa Sand	.251	715	190	.0274
7	Wausau Quartz	.0654	186	702	.00193

DISCUSSION OF RESULTS

One of the major problems in this study was the determination of that unique set of values for the three parameters γ , f and a , which would give the best agreement between the data and the capacitance model (Eq. 28).

This determination was accomplished by a steepest-descent search calculation. The criterion of deviation was the sum of weighted squares of the difference between observed and calculated C/C_0 ,

$$DEV = \sum_{i=1}^{i=6} W_i \left(\Delta \frac{C_i}{C_0} \right)^2 \quad \dots (31)$$

where $\Delta \frac{C_i}{C_0}$ is the difference between the observed

$\frac{C}{C_0}$ and the calculated (Eq. 28) $\frac{C}{C_0}$ at a value of I indicated by i . As indicated by Eq. 31, six points along the concentration profile were employed. Little difficulty with local minimums was encountered in the use of this method.

This search method was also employed to determine unique values of γ and f which would result in the best fit between data and diffusion model solutions (for the three different sets of boundary conditions), Eqs. 12, 14 and 15.

The values of DEV obtained through the search technique from Eqs. 12, 14, 15 and 28 are given in Table 4. This table shows that the capacitance model gave significantly better agreement with data in runs 1, 4, 5 and 7 than was obtained with the diffusion model. No satisfactory match of run 2 or 3 was obtained from any of the equations, while run 6 was matched very well by both the diffusion and capacitance models.

The solid lines of Figs. 1 through 7 show the experimental effluent concentration profiles. The open circles represent the model solution, Eq. 28, while the solid points are calculated from Eq. 14, with I replaced by J . Thus, the solid points repre-

TABLE 2 — CORE PROPERTIES

Core	Permeability Darcys	Particle Size, mm	Length, in.	I. D., in.	Pore Volume, cc	Porosity
No. 1 Wausau Quartz	—	(80-60 Mesh) .18-.25	8.187	1.0	49.4	.467
Ottawa Sand	—	.48-.71	8.156	1.0	36.2	.345
Torpedo Sandstone	1.5-2	—	9.25	1.5	67	.26
Alundum	.5	—	8.0	1.0312	30.2	.274

TABLE 4 — VALUES OF DEVIATION, DEV

Run	Model	Eq.	γ	f	a	DEV
1	Capacitance	(28)	370	.900	.58	.00109
	Diffusion	(12)	91.1	.969	0	.01207
	Diffusion	(14)	90.5	.958	0	.01209
	Diffusion	(15)	103.1	.970	0	.01780
2	Capacitance	(28)	302	.919	1.54	.00432
	Diffusion	(12)	133	1.000	0	.00774
	Diffusion	(14)	133	.995	0	.00728
	Diffusion	(15)	141	1.000	0	.01556
3	Capacitance	(28)	212	.911	1.42	.00420
	Diffusion	(12)	103	1.000	0	.00779
	Diffusion	(14)	100	.995	0	.00683
	Diffusion	(15)	116	1.000	0	.01873
4	Capacitance	(28)	730	.928	.18	.00100
	Diffusion	(12)	320	.948	0	.01710
	Diffusion	(14)	324	.945	0	.01711
	Diffusion	(15)	312	.953	0	.01716
5	Capacitance	(28)	780	.929	.115	.00127
	Diffusion	(12)	484	.940	0	.00851
	Diffusion	(14)	480	.938	0	.00851
	Diffusion	(15)	476	.943	0	.00854
6	Capacitance	(28)	190	.956	.017	.00032
	Diffusion	(12)	178.8	.964	0	.00045
	Diffusion	(14)	178.8	.959	0	.00045
	Diffusion	(15)	172	.973	0	.00046
7	Capacitance	(28)	702	.976	.065	.00019
	Diffusion	(12)	586	.982	0	.00196
	Diffusion	(14)	586	.980	0	.00195
	Diffusion	(15)	582	.984	0	.00196

sent the simple diffusion model with allowance for an amount of dead volume into which diffusion is negligibly slow.

As shown in these figures and Table 5, the $0.5C_0$ concentration appeared significantly before injection of one pore volume, and C/C_0 at one pore volume injected was appreciably above 0.5 for all runs.

Fig. 1 shows that the capacitance model reproduces the Run 1 profile significantly better than the diffusion model. The $0.5C_0$ concentration appeared in the effluent at 0.942 pore volumes injected, and considerable asymmetry is exhibited by the profile. The dispersion coefficient D for run 1 is $0.00057 \text{ sq cm/sec}$ (see Table 3), while Eq. 3 gives, for $\sigma d_p = 0.17$,¹⁵

$$D = 0.5 (0.009) (0.17) = 0.000765 \text{ cm}^2/\text{sec}.$$

The dispersion coefficient of $0.00057 \text{ sq cm/sec}$ for Run 1 as well as the other dispersion coefficient values listed in Table 3 were obtained by matching

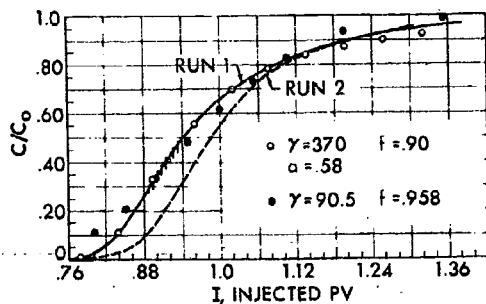


FIG. 1 — CONCENTRATION VS INJECTED PORE VOLUMES FOR RUNS 1 AND 2.

TABLE 5 — BREAKTHROUGH CHARACTERISTICS

Run	I at $C/C_0 = 0.5$	C/C_0 at $I = 1$
1	.942	.65
2	.986	.55
3	.983	.55
4	.934	.775
5	.933	.820
6	.96	.66
7	.982	.65

the mathematical capacitance model to the data. Since this model attributes a certain amount of the mixing to capacitance effects, the dispersion coefficient accounts for only part of the mixing. Thus, these (Table 3) D values should be low in comparison with coefficient values calculated from Eqs. 3 or 14 since those equations attribute all the mixing to the dispersion mechanism alone. In this connection, it is interesting to note that a larger d_p , σ value of 0.54 cm has also been reported for Torpedo sandstone²³ and that value employed in Eq. 3 gives

$$D = 0.5 (0.009) (0.54) = .00242 \text{ cm}^2/\text{sec}.$$

Table 4 lists a γ value of 90.5 determined for Run 1 from the diffusion model, Eq. 14. This γ value gives a dispersion coefficient of

$$D = \frac{\nu L}{\gamma} = \frac{(0.0009) (23.5)}{90.5} = 0.00234 \text{ cm}^2/\text{sec}.$$

This value is in close agreement with the 0.00242 value which is to be expected since they both derive from equations and data wherein the total mixing is attributed to dispersion alone.

The discussion immediately above leads to the first, and perhaps most important, conclusion reached in this study. In laboratory experiments conducted to determine dispersion coefficients (in connection with miscible flooding, for example), the flow velocity ν may be larger and the system length L definitely will be smaller than in the actual field case. Thus, the (laboratory) dimensionless rate group (a) = KL/ν may be sufficiently small to result in a significant contribution to mixing by capacitance effects.

In the field, however, with L typically hundreds of times larger and ν perhaps appreciably smaller, the group (a) may be so large as to effect "instantaneous" mass transfer into stagnant volume, thereby precluding any contribution to mixing from capacitance effects. Thus, a danger arises from attributing the total mixing observed in laboratory flow tests to the dispersion mechanism alone. For the dispersion coefficient thereby obtained may be erroneously large as it accounts for mixing caused by capacitance effects as well as by the dispersion mechanism. For example, in the case of Run 1, the capacitance model yielded a dispersion coefficient of $0.00057 \text{ sq cm/sec}$, a value about one-fourth as large as the $0.00234 \text{ sq cm/sec}$ coefficient yielded by the diffusion model, Eq. 14 which attributes all mixing to dispersion. The rate group (a) was indicated to be 0.58 by the capacitance

model, the run flow velocity was 25 ft/day and core length was 1 ft. Thus, in a field case, the rate group (a) might be about

$$a = \frac{KL}{v} = 0.58 \frac{(500/1)}{(1/25)} = 7250$$

assuming field values of L and v to be 500 ft and 1 ft/day, respectively.* At this (a) value, the capacitance contributes negligibly to mixing so that dispersion in the field would correspond to a dispersion coefficient value of 0.00057 sq cm/sec. The length of the "mixed zone" in the field would be about half that predicted by using the larger 0.00234 sq cm/sec value (since mixed-zone length—e.g., distance between 0.1 and 0.9 C/C_0 values—is proportional to the square root of dispersion coefficient). Thus, the capacitance effect may have little importance in causing asymmetry or mixing at field conditions but nevertheless may be very important in interpreting laboratory data.

The experimental effluent curve for Run 2 is also plotted in Fig. 1 in order to show the rather definite effect of velocity. The observed later breakthrough of the lower concentrations at the higher velocity is in agreement with the "bundle of capillaries" model prediction that, as velocity is increased, the larger pores will experience turbulence and carry relatively less solute, thus delaying breakthrough of the lower concentrations.

The unsatisfactory fits obtained for Runs 2 and 3, shown in Figs. 2 and 3, do not justify attachment

*Obviously, data relating rate constant K to velocity would be required here.

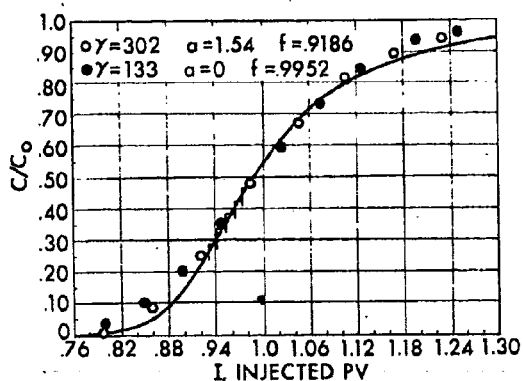


FIG. 2 — CONCENTRATION VS INJECTED PORE VOLUMES FOR RUN 2.

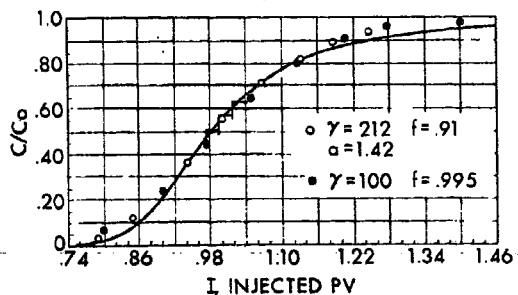


FIG. 3 — CONCENTRATION VS INJECTED PORE VOLUMES FOR RUN 3.

of much significance to the apparent D values, listed in Table 3. Ignoring the poor fit, we would conclude from Table 4 that D was more than linearly proportional to velocity, since $\gamma = \frac{Lv}{D}$ decreased as v increased; also the rate constant K was more than linearly proportional to velocity between rates of 0.009 and 0.0525 cm/sec since $a = KL/v$ increased by over 2.5 as v increased by a factor of 6 between Runs 1 and 2. For velocity above 0.0525 cm/sec, K was roughly proportional to velocity since (a) remained essentially constant as velocity was increased again by a factor of about 4 in Run 3. Substitution of convective mixing for diffusion in stagnant volume of the type shown in Fig. 8b might cause the rate constant to increase sharply with velocity. However, as stated above, the relatively poor predictions attained in Runs 2 and 3 leave the discussion of this paragraph in the realm of almost pure conjecture.

The fact that neither Run 2 nor Run 3 could be matched might be caused by one or more of the following:

1. A mechanism other than bed capacitance is responsible, to a significant extent, for the asymmetry noted.

2. Bed capacitance is the mechanism in question but obeys a transfer law other than the linear form, Eq. 27.

3. Bed capacitance is the mechanism but the discrete pore arrangement of the sandstone requires a finite-stage model (e.g., Deans).

4. Bed capacitance is the mechanism and can be represented by a differential model but different boundary conditions (e.g., Eq. 7) should be used.

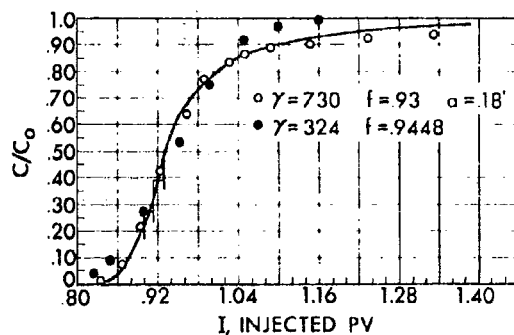


FIG. 4 — CONCENTRATION VS INJECTED PORE VOLUMES FOR RUN 4.

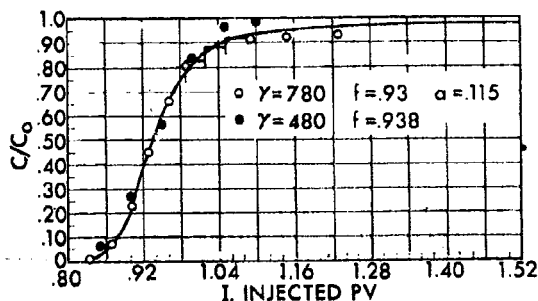


FIG. 5 — CONCENTRATION VS INJECTED PORE VOLUMES FOR RUN 5.

Figs. 4 and 5 show the observed and calculated profiles for the Alundum runs. As noted in Tables 3 and 4, D was essentially proportional to velocity while K was less than linearly proportional to velocity since (a) fell from 0.18 to 0.115 as v was increased by a factor of 12. If K had been constant, (a) would have fallen to about 0.015. The amount of stagnant volume was unaffected by velocity.

Runs 6 and 7, shown in Figs. 6 and 7, resulted in early breakthrough of the 0.5 C_0 concentration and nearly symmetrical profiles. Run 6 was well represented by the diffusion model (with bypassed volume), with little improvement effected by the capacitance model. The dispersion coefficient of 0.0274 sq cm/sec (Table 3) for Ottawa sand compares with a value of

$$D = \frac{(0.251)(20.7)}{178.8} = 0.0291 \text{ cm}^2/\text{sec.}$$

given by the 178.8 γ value (see Table 4) yielded by the diffusion model, Eq. 14. The Wausau quartz Run 7 was reproduced significantly better by the capacitance model than by the diffusion model, as shown in Table 4 and Fig. 7. The D value of 0.00193 compares with

$$D = \frac{(0.0654)(20.8)}{58.6} = 0.00232 \text{ cm}^2/\text{sec.}$$

given by the 58.6 γ value yielded by the diffusion model, Eq. 14. As shown in Table 4, stagnant volumes of about 4.5 and 2.5 per cent are indicated for the Ottawa sand and Wausau quartz sandpacks.

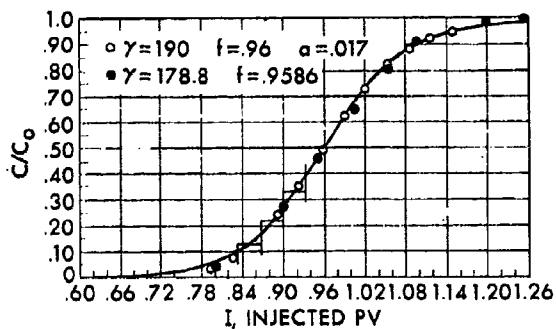


FIG. 6 — CONCENTRATION VS INJECTED PORE VOLUMES FOR RUN 6.

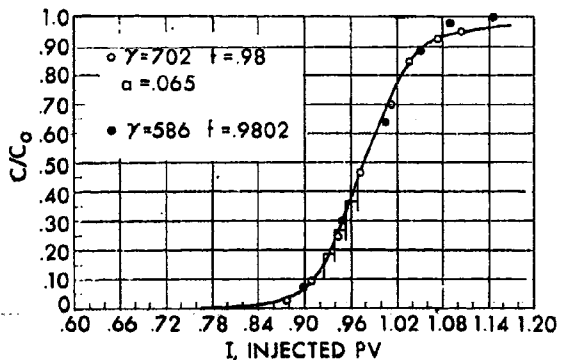


FIG. 7 — CONCENTRATION VS INJECTED PORE VOLUMES FOR RUN 7.

ROLE OF HETEROGENEITY

The effect of heterogeneity in the sandstone depends upon the meaning attached to the term. If microscopic heterogeneity is meant, whereby certain pores are bypassed by flow, then this is precisely the sort of mechanism implied by the capacitance models of Deans or this work. That is, a uniformly distributed stagnant volume is equivalent to microscopic heterogeneity. If, however, macroscopic heterogeneity is meant, in the sense that regions of the order of millimeters are of significantly different permeability or pore structure, then none of the dispersion models allowing analytical solution to date take heterogeneity into account. Core description would be a formidable problem in this case and numerical solution (finite-difference) of the governing equations would be required.

PHYSICAL SIGNIFICANCE OF RATE GROUP KL/v

A physical significance may be attached to the (a) values in Table 4 provided a representation of the assumed stagnant volume is made. Fig. 8 sketches two extremes in the concept of dead-end pore volume, Fig. 8a illustrating the type employed in experiment by Fatt, *et al.*,²² and Fig. 8b representing "dimples" or pits in the walls of otherwise uniform flow networks. If, following Fatt's steady-state fluid flow concept, we suppose the diffusion through the neck leading to the dead space to be steady-state, then

$$V_s \frac{\partial C^*}{\partial t} = \frac{D_0 A}{l} (C - C^*), \dots \dots \dots (32)$$

where V_s is volume of the stagnant space, and A and l are cross-sectional area and length, respectively, of the neck leading to it. Comparison of 32 with 27 gives the equivalence

$$\frac{K}{1-f} = \frac{D_0 A}{V_s l} \text{ OR } a = \frac{D_0 A l (1-f)}{v V_s l} \dots \dots \dots (33)$$

If D_0 is 1.35×10^{-5} sq cm/sec (value for NaCl in water), then the (a) value of 0.58 (Run 1) gives

$$\frac{A}{V_s l} = 164 \text{ cm}^{-2} \dots \dots \dots (34)$$

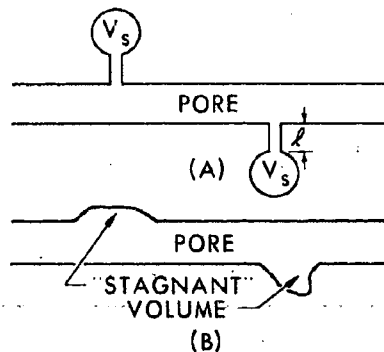


FIG. 8 — IDEALIZED TYPES OF DEAD-END PORE VOLUME.

Microscopic examination of Torpedo sandstone shows irregularly shaped pores of an average diameter of 5 microns. Adjacent pore spaces are separated by a low multiple (e.g., 2 to 4) of the average pore diameter. Let the stagnant volume V_s be spherical with a radius of 2.5 microns, and ℓ be 15 microns; then the neck radius r is given by Eq. 34, where $A = \pi r^2$, as $r = 0.023$ microns. While this seems rather small, little significance can be derived from it without a more detailed knowledge of the structure of arrangement of the pores. An obvious question at this point is whether the assumption of steady-state diffusion through the neck is reasonable. A rough measure of the validity of this assumption is the proximity to C_0 of the concentration at the end of the neck at a time in which the fluid travels a relatively short distance. For example, let fluid of concentration C_0 reach the neck at time zero. In 100 seconds, under Run 1 conditions, the fluid will advance 1 cm. In the same time, the concentration at a distance ℓ (perpendicular to flow) will be, due to diffusion,

$$\frac{C}{C_0} = \operatorname{erfc} \left(\frac{\ell}{2\sqrt{D_0 t}} \right) = \operatorname{erfc} \frac{15 \times 10^{-4} \text{ cm}}{2\sqrt{10^{-5}(100)}} = 0.973,$$

which is sufficiently close to unity that steady-state diffusion through the neck is a valid presumption. Undoubtedly, the concept of a mixed stagnant volume having a uniform concentration C^* is in much greater error than that of steady diffusion through a neck.

The fact that the (a) group values for the unconsolidated sand Runs 6 and 7 are much less than the values for the consolidated cores is not surprising. This would be expected from the fact that the (a) group as given by Eq. 33 is proportional to $A(1-f)/V_s \ell$, which is smaller for these unconsolidated cores for two reasons. First, $(1-f)$ is somewhat smaller for the unconsolidated cores, and second, the group $A/V_s \ell$ has dimensions of $1/\ell^2$ where ℓ is a length characteristic of the media. Since this ℓ will be greater for the "large" particle sandpacks than for the sandstone and Alundum, the value of (a) is further reduced.

VALIDITY OF STAGNANT FILM CONCEPT

The validity of Gottschlich's work¹³ in which bed capacitance is presumed to be in the form of a thin film on pore walls, will now be briefly examined. If diffusion in a film of the order of a few microns in thickness (pores are only 5 microns in diameter) is important as a rate effect, then the concentration C/C_0 by diffusion at a distance of several microns should be considerably less than unity over a period of time in which the fluid travels a short distance. For Run 1, the fluid advanced only 0.1 cm in 10 seconds. In this time diffusion through a film 5 microns thick would have raised the concentration at the far side of the film to $\operatorname{erfc} (5 \times 10^{-4} / 2\sqrt{10^{-5}(10)})$, or to $C/C_0 = 0.972$, assuming a diffusion coefficient of 10^{-5}

sq cm/sec. This indicates that diffusion into a film would be an "instantaneous" type of process at Run 1 conditions, incapable of yielding the extreme asymmetry noted.

DIFFERENTIAL FORM OF DEANS' MODEL

The differential form of Deans' capacitance model, Eq. 21, has been applied to the data of Runs 1 through 7. The value of (a) was obtained from Eq. 24 and the experimental value of C/C_0 at $l = 1$. The term f was then calculated for each of a number of points spanning the effluent profile. The value of Y is simply $ay = a$ since $y = 1$ for all measurements. The value of Z is

$$Z = \frac{a}{1-f} (1-f) \dots \dots \dots (35)$$

Experimental values of C/C_0 and the previously obtained Y value are employed to obtain Z from a table of C/C_0 vs Z and Y (tabular representation of Eq. 22). Eq. 35 and the experimental l values corresponding to the C/C_0 values used then give f for each experimental $(C/C_0, l)$ point. A measure of the "fit" between the model, Eq. 22, and the data, is the constancy of f . The f values determined for Runs 1, 5, 6 and 7 were reasonably constant at 0.9, 0.98, 0.945 and 0.96, respectively; and the corresponding (a) values were 1.05, 0.25, 0.9 and 1.05. Table 6 lists the observed and predicted (from Eq. 22) l values corresponding to selected C/C_0 data points. As shown by Table 6, the major defect of Eq. 22 is its failure to account for the diffuse profile between concentrations of zero and e^{-a} .

TABLE 6 — PREDICTIONS FROM DIFFERENTIAL FORM OF DEAN'S MODEL

Run	C/C_0	Experimental	Eq. 22
1	.35	.90	.90
	.362	.904	.903
	.390	.911	.911
	.64	.994	.995
	.794	1.086	1.081
	.95	1.32	1.281
5	.78	.987	.98
	.831	1.004	1.004
	.870	1.024	1.028
	.908	1.054	1.060
	.959	1.22	1.132
6	.406	.938	.945
	.485	.956	.959
	.593	.982	.982
	.686	1.007	1.006
	.742	1.024	1.024
	.827	1.057	1.061
	.919	1.118	1.128
	.96	1.177	1.189
7	.35	.96	.96
	.362	.961	.961
	.390	.965	.964
	.64	.998	.998
	.794	1.028	1.032
	.95	1.108	1.112

END EFFECTS

The possibility exists that end effects⁷ occurred in the experiments reported herein. One way to test this hypothesis is to repeat the experiments in longer cores. Differences would, however, be expected since a length effect is actually part of the capacitance model. That is, if the group $(a) = KL/\nu$ is in such a range as to cause spreading due to non-instantaneous mass transfer, then a change in length will result in a change in concentration profile through the change in (a) . If K were proportional to ν , then the change in length could not be offset by a change in ν to maintain (a) constant and determine whether L itself has an effect. If end effects are held to cause the asymmetry of Runs 1 through 5, then they are strangely absent in Runs 6 and 7 where symmetry obtained. Also, Carberry and Bretton noted end effects in cores from 1/2 to 3 ft in length only at a Reynold's number in excess of 20. The Reynold's number is about 2 for Run 6, less for the other runs.

Crawford and Atkinson's discussion of Von Rosenberg's data (Ottawa sand) showed that his 2- and 4-ft column data could be obtained closely by superposition of the 1-ft column data. Thus (unless effects cancel) not only does it appear that no end effects were operative in Von Rosenberg's 1-ft column but also that the importance of choice among the boundary conditions 8, 9 and 10 is small (since the superposition effectively "mixes" these conditions).

EFFECT OF BOUNDARY CONDITIONS ON DIFFUSION MODEL SOLUTIONS

Table 1 shows that a significant difference exists between the finite-bed solution 15 and the two infinite-bed solutions 12 and 14, even at γ values as large as 400. Table 4 shows that of the three diffusion model solutions, Eq. 14 achieves, in general, the best agreement with data, followed closely by Eq. 12.

PHYSICAL VALIDITY OF CAPACITANCE MECHANISM

The fact that a capacitance model matches data better than the diffusion model is no "proof" that capacitance with mass transfer is actually present and operative. The simple fact that the capacitance model possesses three parameters, compared with two (including f) for the diffusion model, leads us to expect better predictions from the capacitance model. The discussion beneath Eq. 30 above, however, suggests a relatively simple experimental program for determining whether capacitance is a physical or merely conceptual entity.

If a core is subjected to three displacements, at very low, intermediate, and very high velocities, then the effluent profiles at very low and very high velocities should be nearly symmetrical; and the latter should be displaced to the left of the former on a plot of C/C_0 vs t (with allowance or correction for different values of D at the two velocities). The

concentration profile corresponding to an intermediate velocity should exhibit asymmetry due to the spreading caused by non-instantaneous mass transfer. It is possible, of course, that an entirely different mechanism might produce the same behavior. Until such a mechanism is described, however, the above described behavior would be strong evidence in favor of the physical validity of the capacitance mechanism.

CONCLUSIONS

If stagnant volume is a physical reality, then dispersion coefficients determined by application of a diffusion-type model to laboratory data may be several times too large. Application of a capacitance model to the data would separate the contributions to mixing by capacitance and dispersion mechanisms, yielding a more nearly correct dispersion coefficient for use in field calculations.

Experimental effluent concentration profiles from two consolidated cores exhibit considerable asymmetry and early breakthrough of the 50 per cent concentration. Profiles from two unconsolidated cores show early breakthrough of this concentration but are nearly symmetrical.

The use of a differential capacitance model gives a significantly better match of the data from five of seven runs than can be achieved using the standard diffusion model.

Effluent concentration profiles from two runs in a 500 md Alundum core indicated about 7 per cent of the pore space to be stagnant volume. The rate constant for mass transfer into this volume appeared to be linearly dependent upon velocity. Profiles from a Torpedo sandstone core indicated 10 per cent stagnant volume.

While the data and calculations do not "prove" the existence of stagnant volume, they indicate that the capacitance concept is capable of explaining the observed asymmetry and early breakthrough of the 50 per cent concentration.

The existence of capacitance effects might be verified by comparing effluent concentration profiles from a core over a large velocity range.

ACKNOWLEDGMENT

The authors express their appreciation to the Jersey Production Research Co. for permission to publish the results of this study.

NOMENCLATURE

- a = rate group, KL/ν ,
- C = concentration in mobile fluid,
- C_0 = feed concentration,
- C^* = concentration in stagnant fluid,
- \bar{C} = Laplace transfer of C ,
- d_p = particle diameter, cm,
- \bar{D} = dispersion coefficient, sq cm/sec,
- D_0 = molecular diffusion coefficient, sq cm/sec,
- DEV = criterion of deviation between observed and calculated concentrations (Eq. 31),

F = formation resistivity factor,
 f = fraction of pore space occupied by mobile fluid,
 I_0 = modified Bessel function of first kind, zero order,
 l = pore volumes injected, vt/L ,
 J = l/f ,
 K = rate constant,
 L = core length,
 P_e = Peclet number, vd_p/D ,
 R_e = Reynold's number, $vd_p\rho/\mu$,
 t = time,
 u = superficial velocity (based on core diameter),
 v = average interstitial velocity, cm/sec,
 x = distance from inlet end of core,
 y = dimensionless distance, x/L ,
 Y = ay ,
 $Z = \frac{af}{1-f}(J - y)$,
 σ = number of particles per "mixing cell",
 ϕ = porosity,
 μ = fluid viscosity,
 ρ = fluid density,
 $\gamma = vL/D$.

REFERENCES

1. Lapidus, L. and Amundson, N. R.: *J. Phys. Chem.* (1952) Vol. 56, 984.
2. van Deemter, J. J., Zuiderweg, F. J. and Klinkenberg, A.: *Chem. Eng. Sci.* (1956) Vol. 5, 271.
3. Van Rosenberg, D. U.: *AIChE Jour.* (March, 1956) Vol. 2, 1, 55.
4. McHenry, K. W. and Wilhelm, R. H.: *AIChE Jour.* (March, 1957) Vol. 3, 1, 83.
5. Aronofsky, J. W. and Heller, J. P.: "Diffusion Model to Explain Mixing of Flowing Miscible Fluids in Porous Media", *Trans., AIME* (1957) Vol. 210, 345.
6. Aris, R. and Amundson, N. R.: *AIChE Jour.* (June, 1957) Vol. 3, 2, 280.
7. Carberry, J. J. and Bretton, R. H.: *AIChE Jour.* (Sept., 1958) Vol. 4, 3, 367.
8. Ebach, E. A. and White, R. R.: *AIChE Jour.* (June, 1958) Vol. 4, 2, 261.
9. Turner, G. A.: *Chem. Eng. Sci.* (1958) Vol. 7, 156.
10. Bischoff, K. B. and Levenspiel, O.: *Chem. Eng. Sci.* (1962) Vol. 17, 245.
11. Brenner, H.: *Chem. Eng. Sci.* (1962) Vol. 17, 229.
12. Deans, H. A.: "A Mathematical Model for Dispersion in the Direction of Flow in Porous Media", *Trans., AIME* (1963) Vol. 228, 49.
13. Gottschlich, C. F.: *AIChE Jour.* (Jan., 1963) Vol. 9, 1, 88.
14. Perkins, R. K. and Johnston, O. C.: "A Preview of Diffusion and Dispersion in Porous Media", *Trans., AIME* (1963) Vol. 228, 70.
15. Brigham, W. E., Reed, P. W. and Dew, J. N.: "Experiments on Mixing During Miscible Displacement in Porous Media", *Trans., AIME* (1961) Vol. 222, 213.
16. Taylor, G. I.: *Proc. Royal Soc.* (1953) Vol. 219, 186.
17. Churchill, R. V.: *Modern Operational Mathematics in*

Engineering, McGraw-Hill Book Co., Inc., New York (1944).

18. Carslaw, H. S. and Jaeger, J. C.: *Conduction of Heat in Solids*, Oxford at the Clarendon Press, 2nd Edition (1959).
19. Danckwerts, P. V.: *Chem. Eng. Sci.* (1953) Vol. 2, 1, 1.
20. Thomas, H. C.: *Jour. Am. Chem. Soc.* (1944) Vol. 66, 1664.
21. Klinkenberg, A.: *Ind. & Eng. Chem.* (1947) Vol. 40, 1992.
22. Goodknight, R. C., Klikoff, W. A., Jr. and Fatt, I.: *Jour. Phys. Chem.* (Sept., 1960) Vol. 64, 1162.
23. "A Review of Diffusion and Dispersion in Porous Media", presented at the SPE Production Research Symposium, Univ. of Oklahoma (April 29-30, 1963).

APPENDIX A

SOLVING EQ. 1 FOR TWO SETS OF BOUNDARY CONDITIONS

FOR BOUNDARY CONDITIONS 8

Eq. 1 can be solved for boundary conditions 8 by taking the equation's Laplace transform with respect to t and inverting the solution to the resulting ordinary differential equation. The inversion (which results in Eq. 11 is made by using formula 19, Appendix E of Ref. 18 and formula 11, Appendix B of Ref. 17.

FOR BOUNDARY CONDITIONS 9

By a similar transformation and inversion, Eq. 1 can be solved for conditions 9. After Laplace transformation of Eq. 1, an ordinary differential equation results. Solution of this differential equation and application of conditions 9 yield a transform of the form:

$$\frac{\bar{C}}{C_0} = \frac{1}{s} \frac{e^{-k\sqrt{s+a^2}}}{a+\sqrt{s+a^2}} \dots \dots \dots (A-1)$$

With s replaced by $p - a^2$ this becomes:

$$\frac{\bar{C}}{C_0} = \frac{1}{p-a^2} \frac{e^{-k\sqrt{p}}}{\sqrt{p+a^2}} \dots \dots \dots (A-2)$$

Carslaw and Jaeger give the inverse of

$$\frac{1}{p-a} \frac{e^{-k\sqrt{p}}}{\sqrt{p+h}}$$

with the restriction that $b^2 \neq a$. Of course, this restriction is not met by Eq. A-2, where the terms corresponding to a and b^2 are precisely equal. If, however, the limit as a approaches b^2 of Carslaw and Jaeger's inverse transform is taken, then the result (modified for the substitution $s = p - a^2$) satisfies Eq. 1 and conditions 9. Thus, the solution to Eq. 1 for conditions 9 is obtained rather simply as Eq. 13.

APPENDIX B

SIMILARITY BETWEEN DEANS' MODEL AND DIFFUSION MODEL

Klinkenberg²¹ notes that for $Z > 1$ and $Y > 2$, Eq. 22 becomes, to a close approximation,

$$\frac{C}{C_0} = \frac{1}{2} \left[1 + \operatorname{erf}(\sqrt{Z} - \sqrt{Y}) + \frac{1}{8\sqrt{Z}} + \frac{1}{8\sqrt{Y}} \right] \dots \dots \dots (B-1)$$

For $Z \cong Y$ (i.e., $x \cong vt$ or $y \cong l$) and for large Z and Y , Eq. B-1 reduces to

$$\frac{C}{C_0} = \frac{1}{2} \operatorname{erfc} \left(\frac{\sqrt{a}}{2(1-f)} \frac{y-1}{\sqrt{t}} \right) \dots (B-2)$$

which is nearly identical to the diffusion model solutions 12, 14, and 15 provided that

$$\sqrt{\gamma} = \frac{\sqrt{a}}{1-f} \dots \dots \dots (B-3)$$

or

$$D = \frac{v^2 (1-f)^2}{K} \dots \dots \dots (B-4)$$

Eq. B-4 is the same equivalence developed by Deans through the limiting form of his solution to Eq. 21 for an input concentration pulse. If K is proportional to velocity then B-4 predicts that the dispersion coefficient will be linearly proportional to velocity.

APPENDIX C

SOLUTION OF EQS. 29 AND 30

The Laplace transformation of Eqs. 29 and 30 and the solution of the resulting ordinary differential equation give

$$\frac{\bar{C}(y,s)}{C_0} = 2e^{\frac{\gamma y}{2}} \frac{e^{-\frac{\gamma y}{2} \sqrt{1 + \frac{4s}{\gamma} (1 + a/s + \frac{af}{1f})}}}{s(1 + \sqrt{1 + \frac{4s}{\gamma} (1 + a/s + \frac{af}{1f})})} \dots \dots \dots (C-1)$$

where $\bar{C}(y,s) = \int_0^\infty e^{-sJ} C(y,J) dJ$ is the Laplace transform of C .

As covered in detail by Churchill,¹⁷ the inverse transform of $\bar{C}(y,s)$ is given by

$$C(y,J) = \frac{1}{2\pi i} \lim_{\beta \rightarrow \infty} \int_{\alpha-i\beta}^{\alpha+i\beta} e^{sJ} \bar{C}(y,s) ds, \dots \dots \dots (C-2)$$

where s is the complex quantity $\alpha + iZ$. If $\bar{C}(y,s)$ is expressed in the form

$$\bar{C}(y,s) = p + iq,$$

then C-2 can be written

$$\frac{C(y,J)}{C_0} = \frac{e^{aJ}}{\pi} \int_0^\infty (p \cos ZJ - q \sin ZJ) dZ \dots \dots \dots (C-3)$$

where Z is real. Any $a > 0$ is admissible here and for $y = 1$, $a = 1$, and for C given by C-1, Eq. C-3 becomes:

$$\frac{C(J)}{C_0} = \frac{2e^J}{\pi} \int_0^\infty \frac{e^{\frac{\gamma}{2}(1-\sqrt{\rho} \cos \frac{\theta}{2})}}{a_1^2 + a_2^2} (a_1 \cos(ZJ-w) + a_2 \sin(ZJ-w)) dZ \dots \dots \dots (C-4)$$

where

$$\begin{aligned} \theta &= \tan^{-1} v/u \\ u &= 1 + \frac{4}{\gamma} \left(1 + \frac{ba + a(1+Z^2)}{(1+b)^2 + Z^2} \right) \\ v &= \frac{4Z}{\gamma} \left(1 + \frac{ab}{(1+b)^2 + Z^2} \right) \\ \rho &= \sqrt{u^2 + v^2} \\ b &= af/(1-f) \\ a_1 &= 1 + \sqrt{\rho} \cos \frac{\theta}{2} - Z \sqrt{\rho} \sin \frac{\theta}{2} \\ a_2 &= Z(1 + \sqrt{\rho} \cos \frac{\theta}{2}) + \sqrt{\rho} \sin \frac{\theta}{2} \\ w &= \frac{\gamma}{2} \sqrt{\rho} \sin \frac{\theta}{2} \end{aligned}$$

The solution C-4 was numerically evaluated by Simpson's rule of numerical integration at a "cost" of about 30 seconds of IBM 7072 time for each value of J . ***